Particle fouling in submerged microfiltration membranes: effects of hollow-fiber length and aeration rate

Jeonghwan Kim and Francis A. DiGiano

ABSTRACT

The effects of fiber length and aeration rate on permeate flux decline in tests of a single, submerged, hollow-fiber microfiltration at constant pressure are presented. Without aeration, the initial permeate flux was greater for shorter fiber length (0.3 vs. 0.7 vs. 1 m) at a relatively low feed concentration of bentonite particles (0.1 g/L). However, the same pseudo-steady state in permeate flux was eventually reached for all three fiber lengths as fouling progressed. The fouling rate was greatly reduced by aeration rate for all three fiber lengths. However, the effect was larger as fiber length became shorter. Aeration was not effective for removal of the fouling layer formed near the fiber outlet where the local flux is expected to be highest for the longest fiber length. In the absence of aeration, permeate flux decline was over-predicted slightly in a hollow fiber model by using the specific cake resistance from a small-scale, flat-sheet microfiltration test. The explanation may involve the effect of the axial gradient of pressure drop on local cake resistance for compressible cakes. Aeration changed the structure of the fouling layer such that specific cake resistance was lower than obtained from the flat-sheet test wherein the aeration is not simulated.

Key words | aeration rate, fiber length, fouling, hollow-fiber microfiltration, permeate flux, specific cake resistance, submerged

Jeonghwan Kim
Department of Civil and Environmental Engineering,
Environmental Engineering Program,
Michigan State University,
East Lansing, MI 48823,
USA

Francis A. DiGiano (corresponding author)
Department of Environmental Sciences and Engineering,
University of North Carolina at Chapel Hill,
Chapel Hill,
CB 7431, NC 27599-7431,
USA
Tel.: +1 919 966 2480
Fax: +1 919 966 7911
E-mail: *fran_digiano@unc.edu*

INTRODUCTION

There is considerable interest in the application of the submerged microfiltration (MF) technology in both water and wastewater treatment (Yamamoto *et al.* 1989; Cote *et al.* 1998; Gunder & Krauth 1998). This technology enables integration of particle separation with other processes in the same reactor, thereby resulting in a compact design and a very high quality of product (permeate) water. For example, membranes can be inserted directly into a coagulation basin of a drinking water treatment plant or directly into the aeration basin of an activated sludge wastewater treatment plant known as submerged membrane bioreactors (SMBRs).

The SMBRs are the combined biological and physical process technology integrating suspended growth reactors with membrane filtration. Permeate water is generated by the application of partial vacuum pressure which is less than 1 atmosphere. Aeration is usually used to induce water movement along the fiber in order to minimize the particle fouling on the membrane surface and to provide the oxygen supply to microorganisms. The aeration rate needed to control fouling has been shown to be two or three times larger than to sustain biodegradation (Gander *et al.* 2000; Cornel *et al.* 2003).

Hollow fiber MF membranes have been applied widely in submerged membrane processes because the membranes are self-supporting, backwashable and the fabrication of the modules is relatively simple and economical (Buisson *et al.* 1998; Parameshwaran *et al.* 1999; Chang & Fane 2001; Fane *et al.* 2002; Cui *et al.* 2003). Despite an upsurge of interest in this process, little fundamental information is available to describe how particles deposit on the surface of the hollow fiber MF membrane.

doi: 10.2166/aqua.2006.054

While many research studies of membrane fouling have been conducted with flat-sheet MF membranes, the question arises as to how these results apply to hollow fibers that comprise a large percentage of the commercial market for submerged membranes. The permeate production has been shown to be lower for the hollow-fiber than flat-sheet membrane under the same imposed suction pressure because suction pressure drop varies along the hollow fiber but not along the flat sheet (Gunder & Krauth 1998; Chang & Fane 2001).

A mathematical model was developed to show that flux gradually increases along the length of a hollow fiber (Chang & Fane 2001). The flux near the fiber outlet could be much greater than the average flux for the entire fiber length, especially if the fiber is long and the fiber diameter is small. In fact, the flux near the fiber outlet at startup could even exceed the average critical flux that corresponds to the no-fouling condition; thus particle deposition could still occur in this region (Fane *et al.* 2002; Cui *et al.* 2003; Kim & DiGiano 2006).

Aeration is essential to minimize the accumulation of a foulant layer in submerged membranes. The choice between coarse and fine bubble aeration has been debated (Cui *et al.* 2003; Cornel *et al.* 2003). Better control of fouling is achieved by coarse bubbles because they create a stronger secondary flow of water that limits cake formation and are more effective in promoting local mixing around the fibers (Cui *et al.* 2003; Cornel *et al.* 2003); on the other hand, oxygen mass transfer is more efficient with fine bubbles (Cornel *et al.* 2003). The extent of the improvement in membrane permeability produced by aeration may also depend upon fiber length although relatively little has been reported on this effect to date.

The objective in this study was to test the combined effect of hollow fiber length and aeration on the formation of a cake layer on hollow fibers and thus the decline in specific flux (i.e. flux/pressure). A single MF fiber and model particle suspensions were used in bench-scale tests to facilitate fundamental interpretation of the fouling phenomena. Morphological examinations were included to observe the spatial distribution of foulant accumulation along the fiber length. Because conventional dead-end flat sheet MF membrane tests do not include the effects of fiber length or aeration, it was of interest to investigate whether specific cake resistance determined in such tests still have value in prediction of the fouling rate of submerged hollow fibers.

METHODS

Submerged, single hollow-fiber MF set-up and operation

Hydrophobic, polyvinylidenefluoride (PVDF) hollow-fiber MF membranes (Pall Filtration, USA) with nominal pore size of 0.1 μm, inner radius of 0.3 mm and outer radius of 0.6 mm were used. The schematic of the experimental set-up is shown in Figure 1. A single hollow fiber was formed into a U-shape by bringing two ends together inside a small section of transparent Teflon tubing with inner diameter of 0.63 cm and then sealed with engineering epoxy resin (hardening time less than 10 min) (Shimizu *et al.* 1996). The fiber was immersed vertically into a Plexiglas cylinder with inside diameter of 5 cm and height of 1.7 m. The open sections of the fiber were connected by tubing to the permeate reservoir and to a vacuum pump that was used to drive the flow from the outside to the inside of the fiber as dead-end filtration mode. Fiber lengths of 0.3, 0.7 and 1.0 m were used in this study.

The constant pressure, declining flux mode of filtration was used at a suction pressure of 50 kPa. The weight of water in the permeate reservoir was measured by electric balance (Ohaus Navigator) and the analog signal was sent continuously to a data acquisition system (Balance Talk, Labtronics). Each filtration was conducted for 3 h during which the cumulative permeate volume was recorded over time. Air was introduced from the compressed air tank

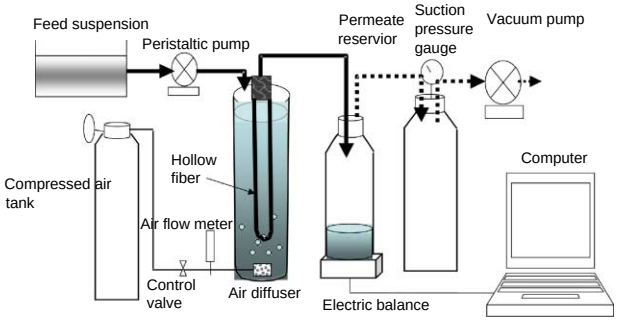

Figure 1 | Schematic of experimental set-up for submerged, hollow-fiber MF (suction mode).

through an air diffuser stone that generated a pattern of coarse air bubbles (about 2 mm as bubble diameter) at the bottom of the reactor. The aeration rate was varied by adjusting the needle valve connected to the air tank. Aeration rate was expressed per unit volume of the reactor. On this normalized basis, the range of aeration rate (0.16–0.78 cm^3 air /cm^3 reactor volume.min) was within the broad range of aeration of the activated sludge system (Ueda *et al.* 1997; Gunder & Krauth 1998; Hong *et al.* 2002) and drinking water treatment applications (Choi *et al.* 2003; Yoon *et al.* 2004).

Model feed suspensions

A bentonite (Fisher Scientific, density = 2660 kg/m^3) suspension with concentration of 0.1 g/L was introduced by peristaltic pump (Manostat) at a rate that was approximately equal to the permeate flow rate. Filtration experiments were also conducted with 0.1 g/L of fluorescent latex particle suspension (Fluoresbrite® Yellow-Green Microspheres, Polyscience, density = 1050 kg/m^3) to investigate the extent of particle deposition along the fiber using image analysis process associated with a confocal laser scanning microscope (CLSM). Bentonite was available as dry form while the fluorescent latex particles were purchased in an aqueous suspension that was subsequently diluted to prepare the desired feed suspension using ultra-pure water. The average sizes in particle diameters using Coulter counter (Multisizer™3 Coulter Counter, Beckman Coulter) were measured to be 0.97 and 0.89 μm for bentonite and latex particles, respectively.

Morphological examinations

Three small segments of the fiber were cut from the open end (fiber outlet or suction source), middle and closed end of the fiber at the end of the hollow-fiber test. Scanning electron microscopy (SEM) (Stereoscan 200, Cambridge) images were made of the outer surface of each of these hollow-fiber segments. The membrane specimen was coated with sputter coating (Hummer X sputter coater, Anatech) with a thin layer of approximately 10 nm of conductive metals (60% of gold and 40% of palladium alloy). A magnification of approximately 5000× was used to obtain the appropriate resolution of the sample.

The fluorescence nature of the fluorescent latex particles enabled use of confocal laser scanning microscopy (CLSM) (Zeiss CLSM 5 Pascal Confocal Laser Scanning Microscope) to examine the extent of deposition of the fluorescent latex particles on the membrane surface. Fluorescence emitted from the fluorescent latex particles that are deposited on the membrane surface is detected by CLSM and the signal is converted into a gray-scale image. An image analysis process (Scion Image) sums up the gray values and subtracts the background to quantify the extent of deposition of fluorescent latex particles on the membrane surface (Savic *et al.* 2003).

Flat sheet membrane test

The flat sheet tests used a cell holder that contained a circular PVDF membrane with a diameter of 4.7 cm and having the same nominal pore size as the hollow-fiber membrane. The effective filtration area was 15.9 cm^2. The suspension was filtered in a dead-end filtration cell (Amicon 8000 series, Millipore) in the batch, unstirred mode. A nitrogen gas tank was used to supply a constant pressure for filtration of the sample. The cumulative permeate volume with filtration time was recorded by electronic balance in order to calculate the specific cake resistance from the classic cake filtration Equation (Chellam *et al.* 1998)

$$\frac{t}{V/A_m} = \frac{\mu\alpha C_0 V}{2\Delta P A_m} + \frac{\mu R_m}{\Delta P} \quad (1)$$

where ΔP is the transmembrane pressure (Pa, kg m/s^2), A_m is the effective membrane surface area (m^2), V is the cumulative permeate volume (m^3), μ is the viscosity of feed suspension (kg/m/s), R_m is the membrane resistance (m^{-1}) and α is the specific cake resistance (m/kg). Data are plotted as $t/V/A_m$ vs. V/A_m and α is determined from the slope from the other known physical parameters that comprise the slope.

Particle compressibility is equally important as specific cake resistance. It is determined by the relationship between α and ΔP and is commonly expressed by a power

law relationship (Tiller & Cooper 1960; Chellam *et al.* 1998):

$$\alpha = \alpha_0 \Delta P^n \tag{2}$$

where α_0 and n are constants that must be determined experimentally. The values of α in this work were determined over a range of ΔP by Equation (1) and the n value was calculated from the slope of logarithmic plots between α and ΔP by Equation (2).

RESULTS AND DISCUSSION

Specific cake resistance and compressibility of particles

The values of α and compressibility for bentonite and fluorescent latex particles are shown in Figure 2. The compressibility of bentonite particles was estimated as about 1.0, indicating highly compressible particles (Kawakatsu *et al.* 1993). Particle deformation that results from compressive pressure acting on bentonite particles within the cake layer can explain compressibility. The values of α were independent upon applied pressure for latex particles, indicating incompressibility. However, a recent study has shown that even rigid incompressible particles can form compressible cakes due to rearrangement of deposits to alter cake structures (Chellam & Wiesner 1998).

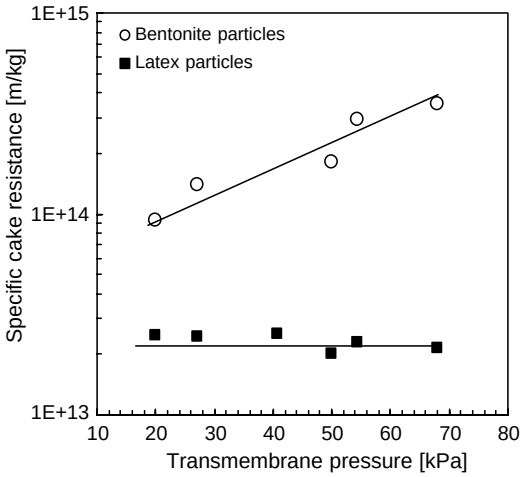

Figure 2 | The specific cake resistance and compressibility by flat-sheet test (feed concentration = 0.1 g/L).

Effects of aeration and fiber length on flux decline

The results of permeate flux decline in submerged, single hollow-fiber MF for three different fiber lengths without aeration are presented in Figure 3 for a bentonite feed concentration of 0.1 g/L at a suction pressure of 50 kPa. The instantaneous flux, which is calculated from the slope of a cumulative volume of filtrate collected vs. time plot divided by the external membrane surface area, is implicitly a fiber-length averaged flux. That is, the variation in flux along the fiber length cannot be measured directly; it could be measured indirectly by measuring the length-average flux in a series of experiments with different fiber lengths. In all of these experiments, the specific flux (flux/pressure) decreased rapidly during the initial period of filtration and then approached pseudo-steady state. During the initial filtration period (< 30 min), the lowest flux corresponded to the longest fiber length. Lower permeate flux could be caused by higher increase in suction pressure drop for longer fiber length than for shorter fiber length under the imposed same suction pressure. However, as time progressed, the flux declined for all three-fiber lengths to about the same value, indicating that the decline in permeate flux appears to be dominated by the fiber length until substantial fouling has occurred.

The reduction in fouling rate due to aeration is shown clearly in Figure 4. Aeration creates a gas–liquid, two-phase flow around the fibers limiting fouling layer, thus enhancing permeate flux (Shimizu *et al.* 1996; Laborie *et al.* 1997; Cabassud *et al.* 2001; Berube & Lei 2005). The positive effect

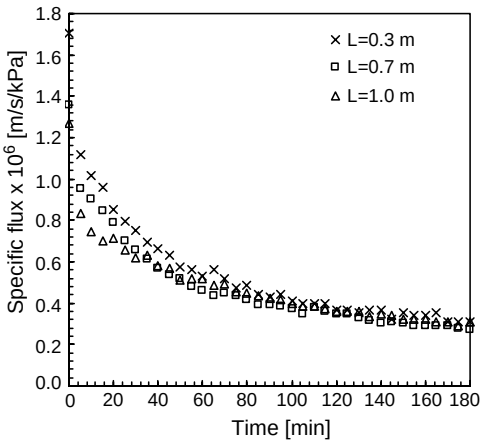

Figure 3 | Permeate flux decline with fiber length without aeration using 0.1 g/L of bentonite suspension at suction pressure of 50 kPa.

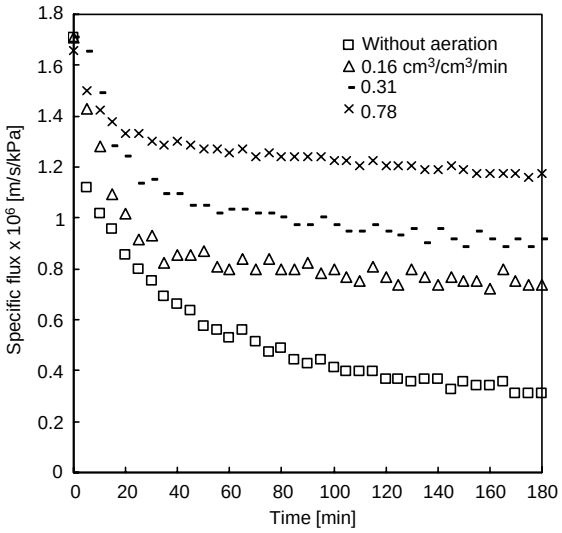

Figure 4 | Specific flux enhancement with aeration rates using 0.1 g/L of bentonite suspension for 0.3 m fiber at suction pressure of 50 kPa.

of aeration on fouling reduction was quantified by plotting the cumulative permeate volume per unit filtration area against filtration time and comparing the result to experiments without aeration. The cumulative filtrate volume for different aeration rates in filtration of 0.1 g/L of bentonite suspension with a 0.3 m fiber length is shown in Figure 5. The increase in filtrate volume produced by aeration at a rate of 0.63 cm^3/cm^3 reactor compared to no aeration was about 160% after a filtration time of 3 h.

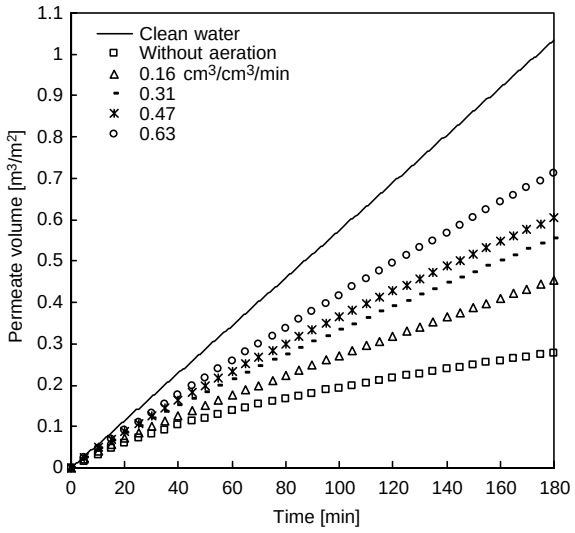

Figure 5 | Relationships between accumulated permeate volume and filtration time for 0.1 g/L of bentonite suspension using 0.3 m fiber with and without aeration (0.16–0.63 cm^3/cm^3.min) at suction pressure of 50 kPa.

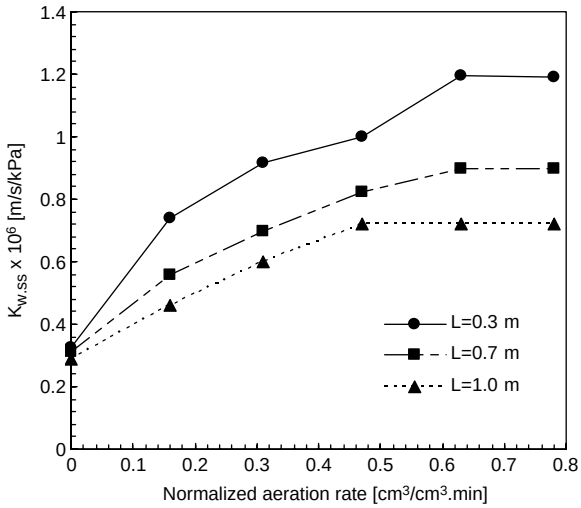

Figure 6 | The effect of aeration rate on pseudo-steady specific flux for 0.1 g/L of bentonite suspension at suction pressure of 50 kPa.

The combined effects of aeration and fiber length on specific flux decline is presented in Figure 6. The specific flux declined at each aeration rate with time but eventually reached an approximately constant value, herein referred to as the pseudo-steady state specific flux, $K_{w.ss}$. The idea of pseudo-steady state is reasonable given existing models of flux decline from the literature (Kilduff *et al.* 2002). Such models are described later in this paper. The specific, pseudo-steady state flux, $K_{w.ss}$ (as measured after 3 h of operation) increased with aeration rate for each fiber length up to a plateau value, which implies that no further reduction in fouling can be achieved beyond this aeration rate. In addition, the results in Figure 6 indicate that the optimal aeration rate is apparently independent of the fiber length. However, the plateau value of $K_{w.ss}$ increases as the fiber length decreases at each optimal aeration rate.

The diminishing benefit of aeration at high rates has been reported in other studies (Laborie *et al.* 1997; Chang & Fane 2001; Hong *et al.* 2002; Berube & Lei 2005). One possible explanation derives from the characteristics of two-phase flow produced by air bubbles traveling through water (Chang & Fane 2001). Two-phase flow promotes local mixing near the membrane surface, thereby enhancing particle back transport; however, the effect in promoting local mixing in secondary flow induced by air bubbles is limited above the critical aeration rate (Hong *et al.* 2002; Cui *et al.* 2003).

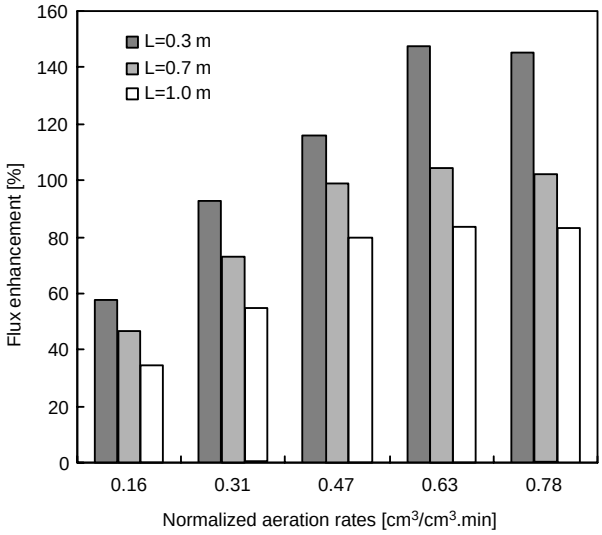

Figure 7 | Pseudo-steady state flux enhancement with aeration rate and fiber length using 0.1 g/L of bentonite suspension at suction pressure of 50 kPa.

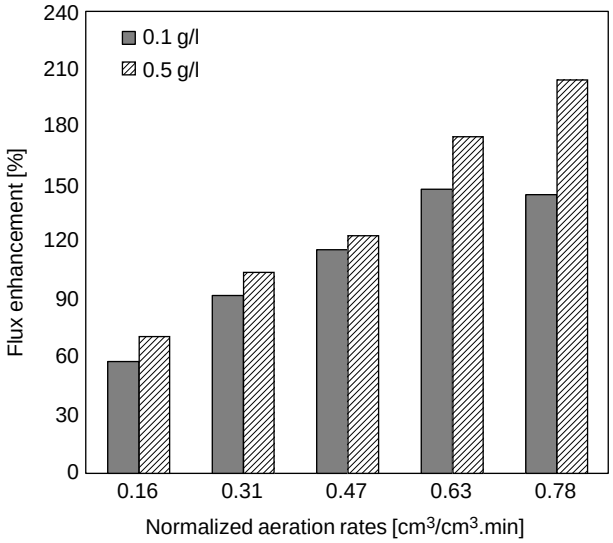

Figure 8 | The effect of bentonite feed concentration on flux enhancement for 0.3 m fiber length at suction pressure of 50 kPa.

The flux enhancement by aeration can also be expressed by $[(K_{\text{w.ss. with aeration}} - K_{\text{w.ss. without aeration}})/K_{\text{w.ss. without aeration}}] \times 100\,(\%)$. The effects of fiber length and aeration rate on $K_{\text{w.ss}}$ are summarized in Figure 7. The shortest fiber length is shown to produce the greatest increase by aeration. Flux enhancement increased with aeration rate for each fiber length but eventually reached a plateau value. In contrast, fiber length had no measurable effect on $K_{\text{w.ss}}$ in the absence of aeration (see also Figure 3).

The fact that aeration rate produced greater control of fouling for short compared to long fibers may be related to the manner in which the fouling layer builds up along the fiber. Given that the longest fiber length has the highest initial particle deposition near the open end of the fiber where the local flux is highest (Fane *et al.* 2002), this region could produce a more compact particle fouling against which aeration may not be very effective (Chu & Li 2005; Kim & DiGiano 2006). In contrast, the initial distribution in flux is much more restricted for shorter fiber length and thus more compact particle fouling may not develop.

Combined effect of particle concentration and aeration on flux decline

The extent of flux enhancement caused by aeration is compared for two feed concentrations of bentonite suspensions in Figure 8. At the highest aeration rate, there was considerably more enhancement in pseudo-steady state flux at higher feed concentration. This result implies that the aeration can be more beneficial when the particle deposition is more severe (Cui & Wright 1996; Sur & Cui 2001).

Microscopic observations of particle fouling along the fiber

The CLSM images taken after 3 h of filtration from the open end, middle and closed end of a 1-m fiber length in the absence of aeration are shown in Figure 9. The CLSM images are presented for the same three locations for filtration with aeration (0.47 cm^3/cm^3 reactor.min) in Figure 10. In both of these experiments, a 0.1 g/L suspension of fluorescent latex particles was filtered at 50 kPa. The CLSM images in Figure 10 were taken after sufficient time to reach a pseudo, steady-state flux (see Figure 4). Significant particle deposition occurred on all three sections of the fiber in the absence of aeration wherein fouling was allowed (Figure 9). As expected, the effect of aeration was to produce far less particle deposition (Figure 10).

The CLSM image analysis process provided a way to quantify the differences in fouling along the fiber length and the effect of aeration as shown in Figure 11. Higher fluorescence intensity at the open than closed end of the fiber means faster accumulation of foulant material. This is consistent with the idea that the flux is highest at the open end of the fiber where the suction pressure is highest

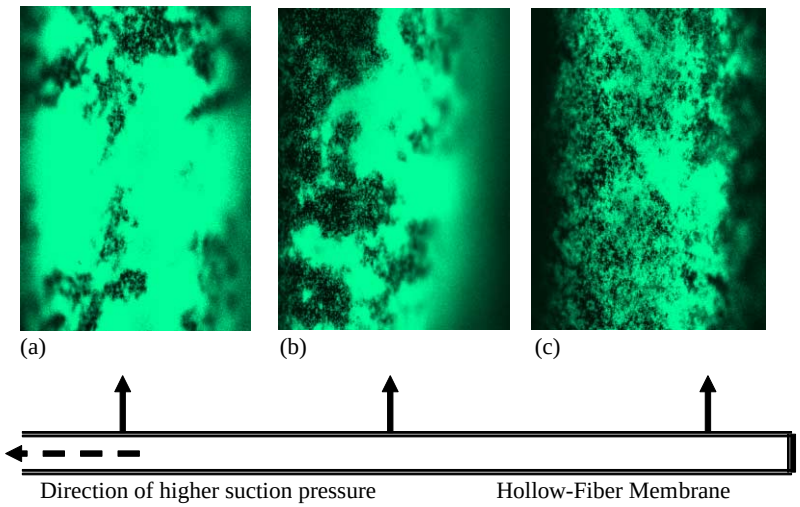

Figure 9 | CLSM images of fluorescent latex particles (0.1 g/L) deposited at open end (a), middle (b) and closed end of the fiber (c) for filtration without aeration (40× magnification, suction pressure = 50 kPa, images were taken after 3 h of filtration time corresponding to 0.63 m^3/m^2 as permeate volume per unit filtration area).

(Carroll & Booker 2000; Chang & Fane 2001); local fouling has been observed to be highest at this location (Chang & Fane 2001; Fane *et al.* 2002). The hypothesis is that the deposition of particles onto the membrane surface start up of filtration is greatest at the open end of the fiber where the suction pressure is highest. As fouling progresses, however, the particle deposition extends to the lower section of the fiber, which originally was characterized by lower than average flux due to having the lowest suction pressure.

The ratio of fluorescence intensity at the open end to that at the closed end of the fiber (R) provides a quantitative measure of the dependence of foulant accumulation on fiber length:

$$R = \frac{(\text{fluorescence intensity})_{\text{open end of fiber}}}{(\text{fluorescence intensity})_{\text{closed end of fiber}}}. \quad (3)$$

The R value is shown in Table 1. The value was considerably higher in submerged membrane tests with aeration than without aeration. For example, R at an aeration rate of 0.31 cm^3/cm^3 reactor.min for a 1-m fiber was about 17 whereas R without aeration was about 1.7.

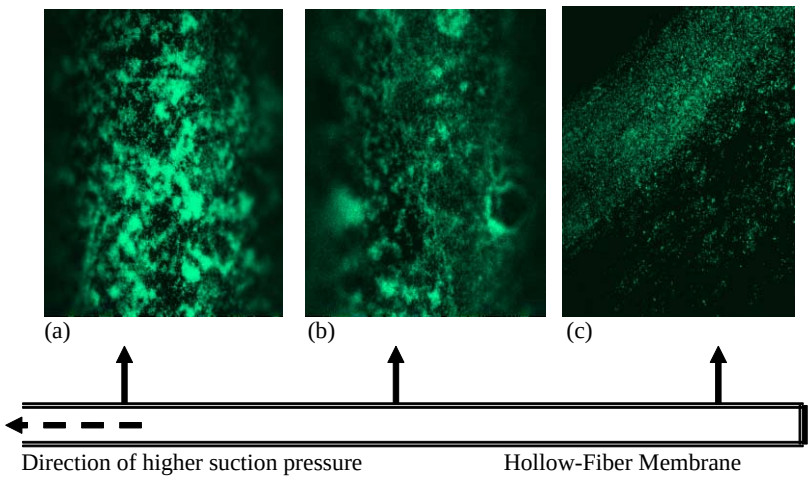

Figure 10 | CLSM images of deposition of fluorescent latex particles (0.1 g/L) at open end (a), middle (b) and closed end (c) of the 1-m fiber at suction pressure of 50 kPa and normalized aeration rate of 0.47 cm^3/cm^3.min (images were taken after 3 h of filtration time corresponding to 0.85 m^3/m^2 as permeate volume per unit filtration area).

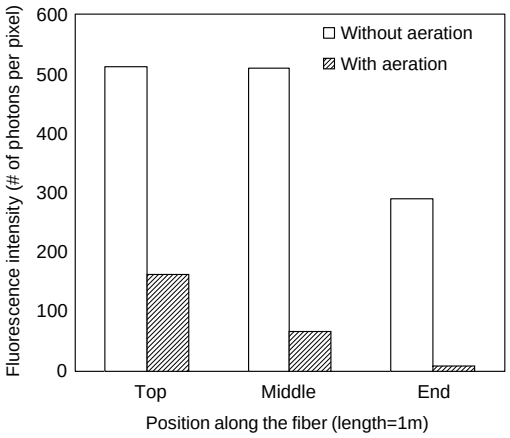

Figure 11 | Fluorescence intensity profile along the fiber length ($L = 1$ m) for fluorescent latex particles (0.1 g/L) using confocal laser scanning microscopy estimated by image analysis process (normalized aeration rate $= 0.31\ cm^3/cm^3.min$, images were taken after 3 h of filtration time).

The R value can also be modified to compare the ratio of fluorescence intensity at the open end to that at the middle of the fiber. For example, the ratio at an aeration rate of $0.31\ cm^3/cm^3.min$ for a 1-m fiber was about 2.5 compared to 1.0 without aeration (also shown in Table 1). The R values between the open end and the middle of the fiber were almost the same without aeration. That is, not only does the foulant material accumulate to a far greater extent without aeration than with aeration (Figure 11), but it is also uniformly distributed along the fiber length.

Higher fluorescence intensity at the open end of the fiber than at the other two regions of the fiber (middle and closed end) even with aeration suggests that the aeration is not completely effective in removing particles that were initially deposited near the open end of the fiber, i.e. where the local flux was initially the highest. By contrast, aeration is more effective at control of particle deposition that occurs later in the operating cycle as flux distribution shifts toward the closed end of the fiber.

Table 1 | Ratio (R) of particle accumulation from open to closed end and from open to middle of 1-m fiber at normalized aeration rate of $0.31\ cm^3/cm^3/min$ based on fluorescence intensity measurements

	***R* for open end/closed end**	***R* for open end/middle**
Without aeration	1.7	1.0
With aeration	17	2.5

Similar patterns of particle fouling were obtained from SEM with bentonite particles deposited at three different positions along a 1-m fiber at an aeration rate of $0.47\ cm^3/cm^3$ reactor.min as shown in Figure 12. The greatest extent of the fouling was found near the open end of the fiber. These results of morphological examinations are consistent with the hypothesis that the differential particle fouling occurs along the fiber length.

Usefulness of specific cake resistance from flat-sheet test in dead-end filtration model without aeration

Data for flat sheet filtration of a 0.1 g/L suspension of bentonite particles at 50 kPa when plotted according to Equation (1) provided a good linear relationship with a correlation coefficient greater than 0.99; α was determined to be 1.8×10^{14} m/kg. This α value was used to predict flux decline for a hollow-fiber membrane at constant pressure in the dead-end filtration model without aeration. The experimental conditions of the single fiber test without aeration approximate the dead-end filtration description.

The form of Darcy's equation for cylindrical geometry of the fiber is given by

$$J = \frac{\Delta P}{\mu\left(\alpha\rho_p\phi_c r_0 \ln\frac{r_0+\delta_c}{r_0} + R_m\right)} \tag{4}$$

where ρ_p is the particle density (kg/m^3), ϕ_c is the solid volume fraction in the cake, δ_c is the cake thickness (m), and r_0 is the outer radius of the hollow fiber (m). The relationship between δ_c and t, as needed in Equation (4), is given by Romero & Davis (1990) as well as by Belfort *et al.* (1994):

$$0.5R_m\left[(r_0+\delta_c)^2 - {r_0}^2\right] + 0.25\alpha\rho_p\phi_c$$
$$r_0\left[2(r_0+\delta_c)^2\ln\left(\frac{r_0+\delta_c}{r_0}\right) - (r_0+\delta_c)^2 + {r_0}^2\right] \tag{5}$$
$$= \frac{\Delta P r_0 \phi_b t}{\mu(\phi_c - \phi_b)}$$

where ϕ_b is the solid volume fraction in feed suspension which is defined as C_0/ρ_p (Chellam *et al.* 1998). Equation (5) shows that $\delta_c = 0$ at $t = 0$ but then the cake layer starts to develop without delay. In this model, the effect of hollow-fiber curvature is included in calculation of the cake area

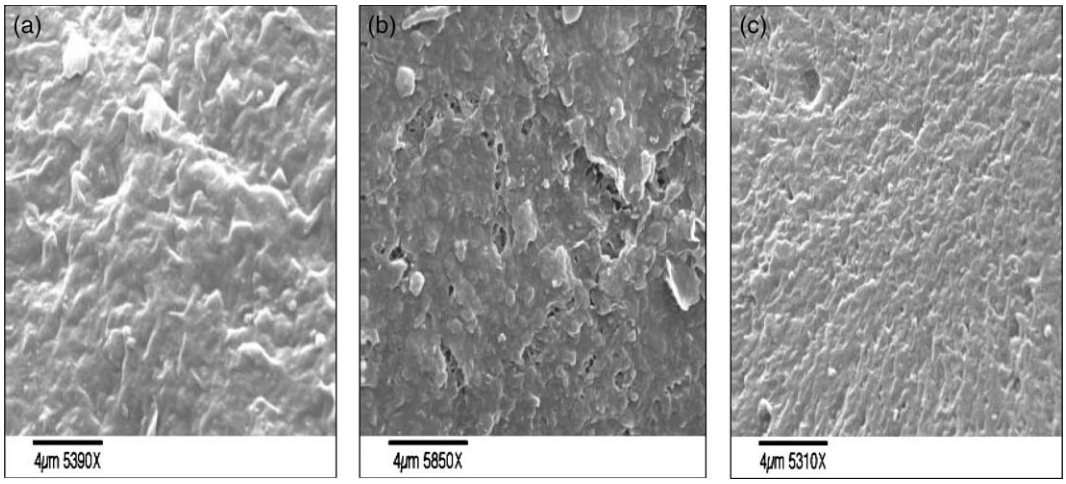

Figure 12 | SEM images of cake surface from 0.1 g/L of bentonite suspension at open end (a), middle (b) and closed end (c) of the 1-m fiber at suction pressure of 50 kPa at normalized aeration rate of 0.47 cm^3/cm^3.min (images were taken after 3 h of filtration time).

(Belfort *et al.* 1994). A mass balance on a radial rather than rectangular geometry is needed to account for the increasing area normal to the flux direction as the fouling layer grows without aeration.

For incompressible, rigid spherical particles, the value of ϕ_c is usually about 0.6–0.65 (Tiller & Yeh 1987). However, ϕ_c could be much lower for irregular bentonite particles because of the tendency to hold water due to their compressible nature that can allow for more open structures (Tiller & Yeh 1987; Yim *et al.* 2002). The difference in weight of the wet and dry bentonite cake (after drying water content) was used to measure ϕ_c by flat sheet test. The resulting value of ϕ_c was very low (0.1), which therefore corresponds to a very high cake porosity of 0.9. However, a similar value of cake solidosity for highly compressible particles has been reported (Tiller & Horng 1983; Tiller & Yeh 1987).

Flux decline as predicted by Equation (4) is compared to experimental data for a fiber length of 0.3 m in Figure 13(a) and a fiber length of 1 m in Figure 13(b). The predicted decline in J was somewhat faster than observed. This discrepancy could be caused by an effect of the axial gradient of pressure drop on local cake resistance for compressible cakes and/or a difficulty in estimating the

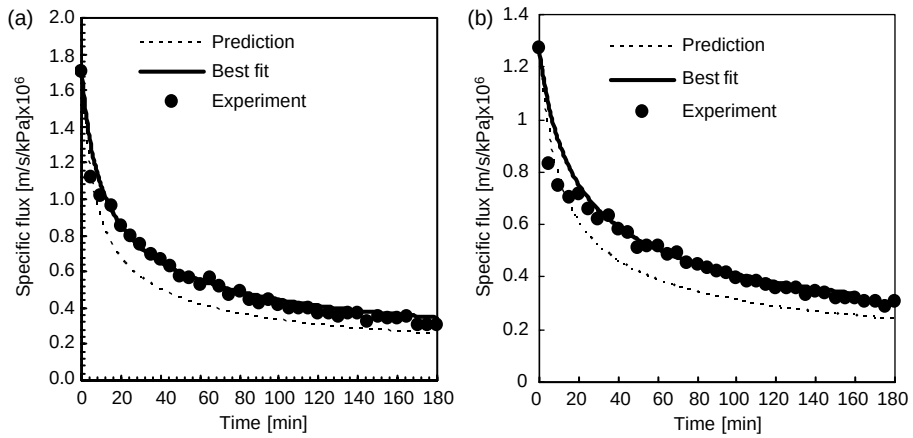

Figure 13 | Model predictions using specific flux decline without aeration: (a) a 0.3-m fiber comparing the α value as determined from flat sheet test (Equation (1)) and with the best fit α as determined from data collected in the submerged fiber test (Equation (4)) and (b) a 1-m fiber using the best fit α from the submerged fiber test with a 0.3-m fiber length.

solidosity of the cake layer which was needed in the model. However, sensitivity testing of Equations (4) and (5) showed that increasing the solidosity from 0.1 to 0.6 had relatively little effect on the rate of flux decline.

The effect of the pressure gradient on local fouling characteristics is important to discuss further. That is, the axial variation in pressure drop along the fiber leads to localized convective forces and, correspondingly, the particle accumulation rate is relatively low along a fraction of the total length. An effect of local suction pressure on α in the hollow fiber configuration should be expected. At lower suction pressure, a less compact fouling layer and thus a more porous cake structure is expected with a correspondingly lower α value. An effect of local suction pressure on α appears consistent with the compressibility of bentonite particles as was shown in Figure 2.

An alternative value of α was calculated by using the experimental data to obtain a best-fit value of α from Equations (4) and (5) by assuming that the other physical parameters remained the same. The best fit α value was 9.5×10^{13} m/kg for the 0.3-m fiber length which is about 47% less than the α value obtained from the small-scale, flat sheet test (1.8×10^{14} m/kg). The same best-fit value of α was then applied to compare the model to the experimental data for a 1-m fiber length (Figure 13(b)). The model over-predicted permeate flux during the initial period of filtration, but gave fairly good agreement for later times.

Usefulness of specific cake resistance from flat-sheet test in dead-end filtration model with aeration

Aeration provides a cross-flow effect by reducing the resistance to filtration and thus increasing permeate flux. The dead-end filtration model (Equation (4)) is therefore no longer appropriate. The effect of cross flow on cake formation in a dead end filtration model has been addressed by Kilduff *et al.* (2002). The rate of change in mass accumulation on the membrane and in cake resistance is reduced by aeration as given by

$$\frac{dR_c}{dt} = \alpha \frac{1}{A_m} \frac{dm}{dt} = \alpha (J - J^*) C_0 \tag{6}$$

where $J*$ is an effective velocity associated with back-transport away from the membrane and R_c is a cake resistance (m^{-1}). The value of $J*$ is interpreted as the pseudo-steady state permeate velocity at which transport of particles toward the membrane surface is balanced by back-transport of particles away from the membrane due to aeration. $J*$ was assumed to be the pseudo-steady state flux at 3 h of filtration time corresponding to each aeration rate in this study.

The two-resistances in series model described by Darcy's equation is

$$J = \frac{\Delta P}{\mu (R_c + R_m)}. \tag{7}$$

Combining Equations (6) and (7) and integrating yields the general solution to predict the solution in permeate flux (Kilduff *et al.* 2002):

$$\frac{1}{J^{*2}} \left\{ \left[\ln \frac{J(J_0 - J^*)}{J_0 (J - J^*)} \right] - J^* \left(\frac{1}{J} - \frac{1}{J_0} \right) \right\} = \frac{\alpha C_0 t}{J_0 R_m}. \tag{8}$$

Equation (8) predicts a decline in J with t that approximates a pseudo-steady state condition as t increases. That is, J is only in the denominator and must continue to decrease with t but at a slow rate. The α value needed in Equation (8) was provided by the flat sheet test, i.e. $\alpha = 1.8 \times 10^{14}$ m/kg. This α value gave the dashed lines shown in Figure 14(a) that are compared to experimental results of submerged filtration for 0.3 m fiber at three different aeration rates. The results show that a faster flux decline based on predictions with the α value from the flat sheet test than was observed experimentally. In addition, the discrepancy between predicted and observed results increases systematically with aeration rate. The conclusion is that flat sheet tests are not useful in predicting the fouling behavior of submerged, hollow-fiber membranes with aeration.

The alternative approach to use of Equation (8) is to find the best fit α value from the experimental data of the specific flux vs. time shown in Figure 14(a). These results are depicted by the solid lines in Figure 14(a). The best fit α values decrease with increasing aeration rate (8.0×10^{13}, 6.3×10^{13} and 4.3×10^{13} m/kg at aeration rates of 0.16, 0.31 and 0.78 cm^3/cm^3 reactor.min, respectively). That is, aeration has the effect of inducing a structural change in the particle deposition layer on membrane surface that decreases specific resistance; this phenomenon has been suggested by others (Cabassud *et al.*

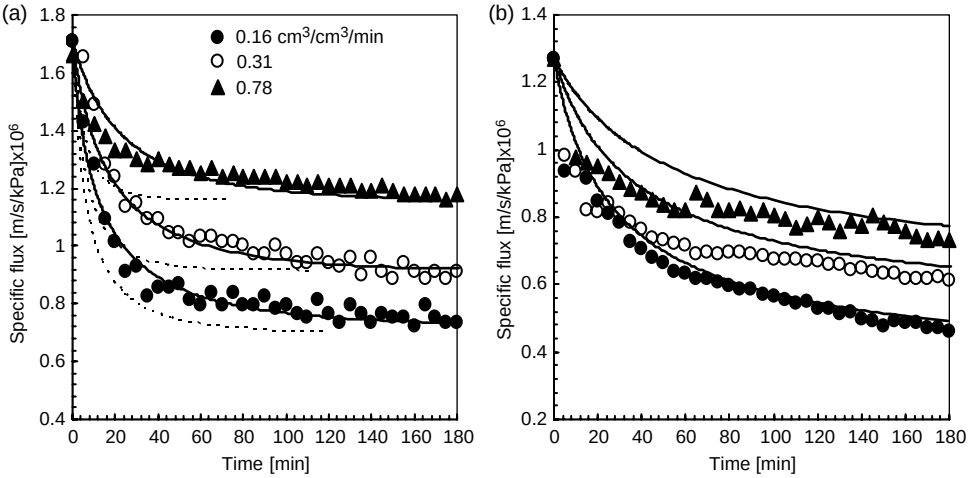

Figure 14 | Model prediction of specific flux decline for three aeration rates: (a) a 0.3-m fiber comparing the α value as determined from flat sheet test (Equation (1)) (dashed line) and with the best fit α as determined from Equation (8) using data collected in submerged fiber tests (solid line) and (b) a 1-m fiber using the best fit α from the submerged fiber test with a 0.3-m fiber length.

2001; Cui *et al.* 2003). Aeration allows us to remove or prevent external cake layer due to secondary flow of mixing and turbulence created by air bubbles in two phase flow. The scouring effect produced by larger particles could also retard transport of smaller particles toward the membrane surface, thus reducing specific cake resistance and enhancing permeate flux. However, further studies are needed to verify this postulation.

Using the best fit values of α determined from the 0.3 m-fiber tests to describe data obtained from 1.0-m fiber tests gave the results presented in Figure 14(b). These α values tended to over-predict the permeate flux, especially during the initial period of filtration. In other words, the specific resistance of the cake layer is somewhat greater for longer fibers at the same aeration rate. This same effect was noted in Figures 6 and 7. All of these results agree with observations by Fane *et al.* (2002) with regard to the importance of initial particle deposition on filtration resistance; this effect is most apparent at longer fiber lengths. The initial filtration resistance could be induced mostly by the fouling layer formed near the open end of the fiber as seen from morphological examinations (Figures 10 and 12), against which aeration may not be very effective.

CONCLUSIONS

All of the experimental observations from these well-controlled, submerged, single hollow-fiber membrane tests point to the effect of the initial flux distribution due to suction pressure drop and its effect on the particle deposition along the fiber and permeate flux characteristics. The suction pressure drop is more pronounced for longer fiber lengths at short filtration times, thus producing lower permeate flux. Without aeration, the difference in fouling rate among fiber lengths dissipated at longer filtration times owing to the leveling out of initial flux distribution and progressive fouling toward lower sections of the fiber.

Aeration greatly reduced the rate of permeate flux decline, although the added benefit was shown to diminish as aeration rate increased. In comparison to relatively more uniform patterns of particle deposition along the fiber at the end of filtration without aeration, the axial features of particle depositions along the fiber was higher with aeration condition. It was observed that particle deposition was more significant near the open end of the fiber than near the middle and closed end of the fiber with aeration. This is because the progress of initial particle deposition formed near the open end of the fiber toward lower sections of the fiber can be retarded by aeration. However, aeration may not be effective to remove initial particle deposition near the open end of the fiber where the local flux is expected to be highest.

The importance of the pressure gradient along a fiber was also shown by attempts to model flux decline from the specific cake resistance that was measured in a small-scale, flat sheet test. The model gave somewhat greater flux

decline than observed in the hollow fiber test without aeration. However, reducing specific cake resistance from the flat sheet by about 47% gave good agreement between the dead-end filtration model and the experimental data. A lower value of specific cake resistance may originate from the axial gradient in pressure forces acting on the particles in hollow-fiber tests. For a bench-scale, flat-sheet test, the pressure drop is distributed evenly across the entire cake layer during filtration period. When the hollow fiber test is conducted at the same pressure with flat sheet test, however, the cake structures could be more porous and fouling rate is relatively low.

Aeration alters the structure of the particle depositions such that the specific cake resistance is lower than obtained from flat-sheet test wherein aeration is not simulated. The initial particle deposition for the longest fiber length may produce a higher filtration resistance than expected from the shortest fiber length. As a result, a higher aeration rate is needed for foulant control in longer than in shorter fibers.

All of the results together suggest limitations in simple bench-scale tests that are used for scale up. Firstly, specific cake resistance from flat sheet tests do not describe the fouling rate of submerged hollow fiber membranes especially those in which aeration is used to control fouling. Secondly, the aeration rate for optimal fouling control based on short fiber lengths, as are typically used in many bench-scale tests, may not apply to full-scale fiber lengths. More definitive conclusions about difficulties in scale up, however, cannot be made without first addressing the question of hydrodynamic similitude in the design of bench-scale experiments by use of dimensional analysis.

ACKNOWLEDGEMENTS

The authors would like to thank Water Environment Research Foundation for the financial support and Pall Filtration for providing membrane materials. Dr. Bagnell, Director of Microscopy Services Laboratory at Department of Pathology and Laboratory Medicine, University of North Carolina at Chapel Hill, is gratefully acknowledged for helping to interpret CLSM images.

REFERENCES

Belfort, G., Davis, R. H. & Zydney, A. L. 1994 The behavior of suspensions and macromolecular solutions in crossflow microfiltration. *J. Membrane Sci.* **96**, 1–58.

Berube, P. R. & Lei, E. 2005 The effect of hydrodynamic conditions and system configurations on the permeate flux in a submerged hollow fiber membrane system. *J. Membrane Sci.* **271**(1–2), 29–37.

Buisson, H., Cote, P., Praderie, M. & Pailard, H. 1998 The use of immersed membranes for upgrading wastewater treatment plants. *Wat. Sci. Technol.* **37**(9), 89–95.

Cabassud, C., Laborie, S., Durand-Bourlier, L. & Laine, J. M. 2001 Air sparging in ultrafiltration hollow fibers: Relationship between flux enhancement, cake characteristics and hydrodynamic parameters. *J. Membrane Sci.* **181**(1), 57–69.

Carroll, T. & Booker, N. A. 2000 Axial features in the fouling of hollow fiber membranes. *J. Membrane Sci.* **168**(1–2), 203–212.

Chang, S. & Fane, A. G. 2001 The effect of fiber diameter on filtration and flux distribution-relevance to submerged hollow fiber modules. *J. Membrane Sci.* **184**(2), 221–223.

Chellam, S., Jacangelo, J. G. & Bonacquisti, T. P. 1998 Modeling and experimental verification of pilot plant scale hollow fiber, direct flow microfiltration with periodic backwashing. *Environ. Sci. Technol.* **32**(1), 75–81.

Chellam, S. & Wiesner, M. R. 1998 Evaluation of crossflow filtration models based on shear-induced diffusion and particle adhesion: complications induced by feed suspension polydispersivity. *J. Membrane Sci.* **138**(1), 83–97.

Choi, S. I., Kim, S. G., Yoon, J. Y., Ahn, K. H. & Lee, S. H. 2003 Particle behavior in air agitation in submerged membrane filtration. *Desalination* **158**, 181–188.

Chu, H. P. & Li, X. 2005 Membrane fouling in a membrane bioreactor (MBR): sludge cake formation and fouling characteristics. *Biotechnol. Bioengng.* **90**(3), 323–331.

Cornel, P., Wagner, M. & Krause, S. 2003 Investigation of oxygen transfer rates in full-scale membrane bioreactors. *Wat. Sci. Technol.* **47**(11), 313–319.

Cote, P., Herve, B. & Matthieu, P. 1998 Immersed membranes activated sludge process applied to the treatment of municipal wastewater. *Wat. Sci. Technol.* **38**(4–5), 437–442.

Cui, Z. F., Chang, S. & Fane, A. G. 2003 The use of gas bubbling to enhance membrane processes. *J. Membrane Sci.* **221**(1–2), 1–35.

Cui, Z. F. & Wright, K. I. T. 1996 Flux enhancement with gas sparging in downwards crossflow ultrafiltration: performance and mechanism. *J. Membrane Sci* **117**(1–2), 109–116.

Fane, A. G., Chang, S. & Chardon, E. 2002 Submerged hollow fiber membrane module-design options and operational considerations. *Desalination* **146**(1–3), 231–236.

Gander, M. A., Jefferson, B. & Judd, S. J. 2000 Membrane bioreactors for use in small wastewater treatment plants: membrane materials and effluent quality. *Wat. Sci. Technol* **41**(1), 205–211.

Gunder, B. & Krauth, B. K. 1998 Replacement of secondary clarification by membrane separation-results with plate and hollow fiber modules. *Wat. Sci. Technol.* **38**(4–5), 383–393.

Hong, S. P., Bae, T. H., Tak, T. K., Hong, S. K. & Randall, A. 2002 Fouling control in activated sludge submerged hollow fiber membrane bioreactor. *Desalination* **143**(3), 219–228.

Kawakatsu, K., Nakao, S. & Kimura, S. 1993 Effects of size and compressibility of suspended particles and surface pores size of membrane on flux in crossflow filtration. *J. Membrane Sci.* **81**(1–2), 173–190.

Kilduff, J. E., Mattaraj, S., Sensibaugh, J., Pieracci, J. P., Yuan, Y. & Belfort, G. 2002 Modeling flux decline during nanofiltration of NOM with poly(arylsulfone) membranes modified using UV-assisted graft polymerization. *Environ. Engng. Sci.* **19**(6), 477–495.

Kim, J. H. & DiGiano, F. A. 2006 Defining critical flux in submerged membranes: Influence of length-distributed flux. *J. Membrane Sci.* **280**(1–2), 752–761.

Laborie, S., Cabassud, C., Durand-Bourlier, L. & Laine, J. M. 1997 Flux enhancement by a continuous tangential gas flow in ultrafiltration hollow fibers for drinking water production:effect of slug-flow on cake structure. *Filtr. Sep.* **34**(8), 887–891.

Parameshwaran, K., Visvanathen, C. & Ben Aim, R. 1999 Membrane as solid/liquid separator and air diffuser in bioreactor. *J. Environ. Engng.* **125**, 825–834.

Romero, C. A. & Davis, R. H. 1990 Transient model of crossflow microfiltration. *Chem. Engng. Sci.* **45**(1), 13–25.

Savic, R., Luo, L., Eisenberg, A. & Maysinger, D. 2003 Micellar nanocontainers distribute to defined cytoplasmic organelles. *Science* **300**, 615–618.

Shimizu, Y., Okuno, Y. I., Uryu, K., Ohtsubo, S. & Watanabe, A. 1996 Filtration characteristics of hollow fiber microfiltration membranes used in membrane bioreactor for domestic wastewater treatment. *Wat. Res.* **30**(10), 2385–2394.

Sur, H. W. & Cui, Z. F. 2001 Experimental study on the enhancement of yeast microfiltration with gas sparging. *J. Chem. Technol.* **76**, 477–484.

Tiller, F. M. & Cooper, H. R. 1960 The role of porosity in filtration: IV Constant pressure filtration. *AIChE J.* **6**(4), 595–601.

Tiller, F. M. & Horng, L. 1983 Hydraulic deliquoring of compressible filter cakes. *AIChE J.* **29**(21), 297–305.

Tiller, F. M. & Yeh, C. S. 1987 The role of porosity in filtration: Part XI: Filtration followed by expression. *AIChE J.* **33**(8), 1241–1256.

Ueda, T., Hata, K., Kikuoka, Y. & Seino, O. 1997 Effects of aeration on suction pressure in a submerged membrane bioreactor. *Wat.Res.* **31**(3), 489–494.

Yamamoto, K., Hiasa, M., Mahmood, T. & Matuso, T. 1989 Direct solid-liquid separation using hollow fiber membrane in an activated sludge aeration tank. *Wat. Sci. Technol.* **21**, 43–54.

Yoon, S. H., Kim, H. S. & Yeom, I. T. 2004 Optimization model of submerged hollow fiber membrane modules. *J. Membrane Sci.* **234**(1–2), 147–156.

Yim, S. S., Song, Y. M. & Chun, S. J. 2002 Study on measurement of average specific cake resistance in cake filtration of particulate suspension and sedimentation floc. *J. Korean Chem. Eng* **40**(3), 330–339.

First received 13 March 2006; accepted in revised form 12 July 2006